Inorganic Chemistry
Article

Inorg. Chem. **2010**, *49*, 5231–5240 **5231**
DOI: 10.1021/ic1003963

Disubstituted 1,8-Diamidonaphthalene Ligands as a Flexible, Responsive, and Reactive Framework for Tantalum Complexes

Nathalie Lavoie,[†] Serge I. Gorelsky,[†] Zhixian Liu,[†] Tara J. Burchell,[†] Glenn P. A. Yap,[‡] and Darrin S. Richeson*[,†]

[†]*Department of Chemistry and the Center for Catalysis Research and Innovation, University of Ottawa, Ottawa, Ontario, Canada K1N 6N5, and* [‡]*Department of Chemistry and Biochemistry, University of Delaware, Newark, Delaware 19716*

Received February 26, 2010

Deprotonated N,N′-disubstituted 1,8-diaminonaphthalenes (R_2DAN^{2-}; R = $(CH_3)_2CH$, C_6H_5, 3,5-$Me_2C_6H_3$) were incorporated into Ta(V) complexes employing two methods. The direct proton transfer reaction of the parent amine, 1,8-$(RNH)_2C_{10}H_6$, with $TaMe_3Cl_2$ led to elimination of methane and formation of $TaCl_3$[1,8-$(RN)_2C_{10}H_6$] (**1**, **2**). Reaction of the dilithiated amido species, Li_2R_2DAN, with $TaMe_3Cl_2$ or [$Ta(NEt_2)_2Cl_3$] yielded $TaMe_3$-[1,8-$(RN)_2C_{10}H_6$] (**3**, **4**) and $TaCl(NEt_2)_2$[1,8-$(RN)_2C_{10}H_6$] (**5**, **6**), respectively. X-ray structural studies of these complexes revealed the flexible coordination behavior of R_2DAN^{2-} by demonstrating that the ligand bonded to Ta with a coordination array dependent on the identity of the other ligands bonded to tantalum. Computational analysis of these complexes confirmed that the energetic components for binding of R_2DAN^{2-} to these TaX_3^{2+} fragments were dominated by the electronic features of the metal fragment. Chemical transformations of the bound ligand were evaluated by reaction of compounds **5** and **6** with $LiNMe_2$ and MeLi. Simple metathesis products $Ta(NEt_2)_2NMe_2$-[1,8-(^{i}PrN)$_2C_{10}H_6$] (R = ^{i}Pr **7**, R = 3,5-$Me_2(C_6H_3)$ **8**) were obtained from reactions with $LiNMe_2$. In contrast, when the R group of the DAN ligand was ^{i}Pr, reaction with MeLi ultimately led to activation of the isopropyl group and formation of the metallaziridine [κ^3-(Me_2CN)(^{i}PrN)$C_{10}H_6$]$Ta(NEt_2)_2$ (**9**) species via the elimination of methane.

Introduction

Exploring ligand−metal bonding and the associated impact on the stability and reactivity of metal complexes is a central theme in inorganic and organometallic chemistry. With d^0, early transition metal complexes, amido ligands have a well-established position, and the role of such species in a host of small molecule transformations continues to stimulate interest in this area.[1,2] Expanding the investigation of new ligands remains an important endeavor with the goal of revealing both fundamental and applied impact of the ligand in chemical transformation and catalysis. One of our general interests, the design and implementation of rigid chelating ligands with delocalized π-electrons, led us to investigate the utilization of a family of diamido ligands, $\{1,8\text{-}(RN)_2C_{10}H_6\}^{2-}$ (**A**, R_2DAN^{2-}), in transition metal complexes.[3] In particular, we reported the reaction of 1,8-$(^i$PrNH$)_2C_{10}H_6$ with $TaMe_3Cl_2$ to produce an unusual metallaaziridine complex, $\{[\kappa^3\text{-}(Me_2CN)(^i\text{PrN})C_{10}H_6]TaCl_2\}_2$ (**B**).[3a] This species apparently arose from a σ-bond metathesis involving the ipso-CH function of the isopropyl substituents of the diamidonaphthalene ligand and elimination of methane from a Ta-Me function, yielding this novel tridentate trianionic ligand, $[(Me_2CN)(Me_2CHN)C_{10}H_6]^{3-}$. We now report on the elaboration of this chemistry along two avenues. The first involves changing the N-substituents of the $\{1,8\text{-}(RN)_2C_{10}H_6\}^{2-}$ ligand in an effort to control the reactivity of these groups when this scaffold is bonded to tantalum. The second explores the influence on the bonding and reactivity of the R_2DAN^{2-} through variation of the remaining ligands bonded to Ta. Through these efforts we

*To whom correspondence should be addressed. E-mail: darrin@uottawa.ca.

(1) (a) Decams, J. M.; Daniele, S.; Hubert-Pfalzgraf, G. L.; Vaissermann, J.; Lecocq, S. *Polyhedron* **2001**, *20*, 2405. (b) Ketterer, A. N.; Fan, H.; Blackmore, J. K.; Yang, X.; Ziller, W. J.; Baik, M.-H.; Heyduk, A. F. *J. Am. Chem. Soc.* **2008**, *130*, 4364. (c) Ison, E. A.; Ortiz, C. O.; Abboud, K.; Boncella, J. M. *Organometallics* **2005**, *24*, 6310. (d) Ketterer, A. N.; Ziller, W. J.; Rheingold, L. A.; Heyduk, A. F. *Organometallics* **2007**, *26*, 5330. (e) Ison, A. E.; Abboud, A. K.; Ghiviriga, I.; Boncella, J. M. *Organometallics* **2004**, *23*, 929. (f) Cameron, M. T.; Ghiviriga, I.; Abboud, A. K.; Boncella, J. M. *Organometallics* **2001**, *20*, 4378. (g) Aoyagi, K.; Gantzel, K. P.; Kalai, K.; Tilley, T. D. *Organometallics* **1996**, *15*, 923.

(2) For selected reviews see: (a) Britovsek, G. J. P.; Gibson, V. C.; Wass, D. F. *Angew. Chem., Int. Ed.* **1999**, *38*, 428, and references therein. (b) Arndtsen, B. A.; Bergman, R. G.; Mobley, T. A.; Peterson, T. H. *Acc. Chem. Res.* **1995**, *28*, 154, and references therein.. (c) Berresford, D. J.; Bolm, C.; Sharpless, K. B. *Angew. Chem., Int. Ed. Engl.* **1995**, *34*, 1059, and references therein. (d) Negishi, E.; Takahashi, T. *Acc. Chem. Res.* **1994**, *27*, 124, and references therein. (e) Tilley, T. D. *Acc. Chem. Res.* **1993**, *26*, 22, and references therein.

(3) (a) Bazinet, P.; Yap, G. P. A.; Richeson, D. S. *Organometallics* **2001**, *20*, 4129. (b) Lavoie, N.; Ong, T. G.; Gorelsky, S. I.; Korobkov, I.; Yap, G. P. A.; Richeson, D. S. *Organometallics* **2007**, *26*, 6586.

Published on Web 05/14/2010

Scheme 1

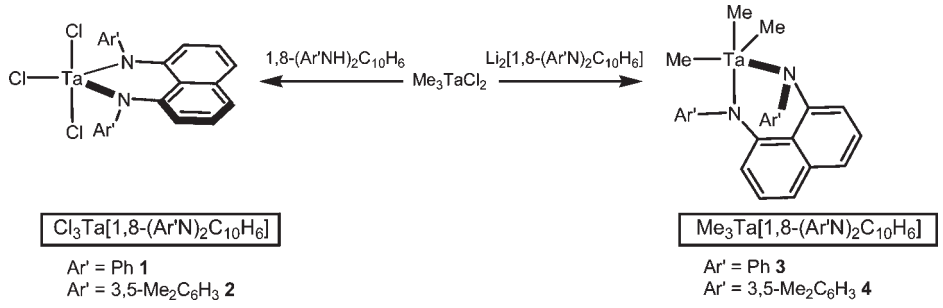

Table 1. Selected Crystal Data and Structure Refinement Parameters for $TaCl_3[1,8\text{-}(PhN)_2C_{10}H_6]$ (**1**), $TaMe_3[1,8\text{-}(PhN)_2C_{10}H_6]$ (**3**), $TaNEt_2Cl[1,8\text{-}(^iPrN)_2C_{10}H_6]$ (**5**), and $TaNEt_3NMe[1,8\text{-}(^iPrN)_2C_{10}H_6]$ (**7**)

	1	**3**	**5**	**7**
empirical formula	$C_{25}H_{23}Cl_3N_2Ta$	$C_{25}H_{25}N_2Ta$	$C_{24}H_{40}ClN_4Ta$	$C_{26}H_{46}N_5Ta$
formula mass	638.75	534.42	601.00	609.63
temp (K)	203(2)	203(2)	201(2)	293(2)
λ (Å)	0.71073	0.71073	0.71073	0.71073
cryst syst	triclinic	triclinic	monoclinic	triclinic
a (Å)	7.906(5)	10.5074(11)	14.8426(12)	10.5712(12)
b (Å)	12.406(8)	10.5509(11)	11.4911(9)	10.6469(12)
c (Å)	13.806(9)	11.9869(13)	16.5518(13)	14.3310(17)
α (deg)	70.028(7)	96.708(2)	90	74.850(2)
β (deg)	85.467(7)	113.601(2)	113.9450(10)	73.189(2)
γ (deg)	78.172(7)	113.073(2)	90	65.1710(10)
V (Å^3)	1245.7	1059.64(19)	2580.1(4)	1383.0(3)
Z	2	2	4	2
ρ(calc) (Mg/m^3)	1.703	1.675	1.547	1.464
μ (mm^{-1})	4.748	5.198	4.381	3.995
absorp corr		semiempirical from equivalents		
final R indices $[I > 2\sigma(I)]$				
$R_1{}^a$	0.0581	0.0372	0.0367	0.0446
$wR_2{}^b$	0.1138	0.1674	0.0762	0.1065

$^a R_1 = \sum||F_o|-|F_c||/\sum|F_o|$. $^b wR_2 = (\sum w(|F_o|-|F_c|)^2/\sum w(|F_o|^2)^{1/2}$.

demonstrate the versatility and flexibility of this ligand class in bonding with metal centers, its responsiveness to the electronic demands of the metal center, and conditions to provoke reaction and CH activation.

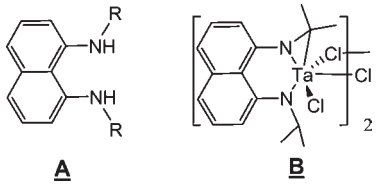

Results and Discussion

Synthesis and Characterization of R_2DAN^{2-} Complexes of Ta(V). The introduction of the dianionic 1,8-diamidonaphthalene ligand, R_2DAN^{2-}, into the coordination sphere of a metal complex can be achieved using two complementary approaches. The first avenue involves the direct reaction of the parent amine, $1,8\text{-}(RNH)_2C_{10}H_6$ (R_2DANH_2), with a metal complex possessing two basic ligands that are capable of undergoing a proton transfer reaction. Elimination of the metal-bound ligand results in incorporation of dianion R_2DAN^{2-} into the metal coordination sphere. A second method involves a two-step process that first deprotonates R_2DANH_2 with butyllithium to generate a dilithiated amido species, Li_2R_2DAN. A subsequent metathesis reaction between this reagent and a dichloro metal complex would incorporate the R_2DAN^{2-} ligand onto the metal center along with elimination of two equivalents of LiCl.

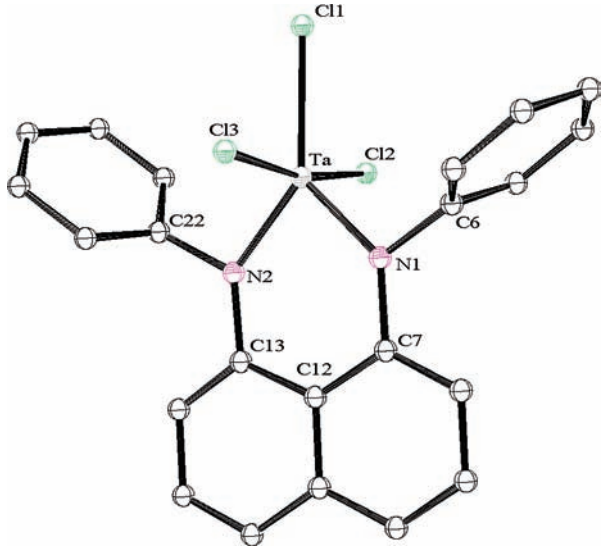

Figure 1. Thermal ellipsoid plot showing the molecular structure and partial atom numbering scheme for $TaCl_3[1,8\text{-}(PhN)_2C_{10}H_6]$ (**1**). Ellipsoids are drawn at 20% probability. Hydrogen atoms have been omitted for clarity.

Table 2. Selected Bond Lengths and Angles for $TaCl_3[1,8\text{-}(PhN)_2C_{10}H_6]$ (**1**), $TaMe_3[1,8\text{-}(PhN)_2C_{10}H_6]$ (**3**), $TaNEt_2Cl[1,8\text{-}(^iPrN)_2C_{10}H_6]$ (**5**), and $TaNEt_3NMe[1,8\text{-}(^iPrN)_2C_{10}H_6]$ (**7**)

Bond Lengths (Å)

1		**3**		**5**		**7**	
Ta−N(1)	1.892(8)	Ta−N(1)	2.064(7)	Ta(1)−N(1)	1.938(5)	N(1)−Ta(1)	2.064(18)
Ta−N(2)	1.931(9)	Ta−N(2)	1.954(7)	Ta(1)−N(2)	2.084(5)	N(2)−Ta(1)	2.04(3)
Ta−Cl(3)	2.393(3)	Ta−C(23)	2.120(10)	Ta(1)−N(3)	1.948(5)	N(4)−Ta(1)	1.899(10)
Ta−Cl(2)	2.396(3)	Ta−C(25)	2.153(11)	Ta(1)−N(4)	1.965(5)	N(5)−Ta	1.987(10)
Ta−Cl(1)	2.414(3)	Ta−C(24)	2.181(10)	Ta(1)−Cl(1)	2.468(2)	N(3)−Ta	2.086(10)
N(2)−C(13)	1.432(12)	N(2)−C(22)	1.397(10)	N(1)−C(1)	1.443(8)	N(1)−C(1)	1.405(15)
N(2)−C(22)	1.422(12)	N(2)−C(13)	1.420(10)	N(1)−C(11)	1.491(8)	N(1)−C(11)	1.50(2)
N(1)−C(7)	1.445(12)	N(1)−C(7)	1.430(9)	N(2)−C(9)	1.391(8)	N(2)−C(10)	1.418(15)
N(1)−C(6)	1.450(13)	N(1)−C(6)	1.430(10)	N(2)−C(14)	1.488(8)	N(2)−C(14)	1.45(3)

Bond Angles (deg)

1		**3**	
C(7)−N(1)−C(6)	121.4(8)	C(7)−N(1)−C(6)	114.8(7)
C(7)−N(1)−Ta	136.1(7)	C(7)−N(1)−Ta	111.2(5)
C(6)−N(1)−Ta	102.4(6)	C(6)−N(1)−Ta	133.4(5)
C(22)−N(2)−C(13)	123.8(9)	C(22)−N(2)−C(13)	120.5(7)
C(22)−N(2)−Ta	99.9(6)	C(22)−N(2)−Ta	135.7(6)
C(13)−N(2)−Ta	134.9(7)	C(13)−N(2)−Ta	101.0(5)
N(1)−Ta−N(2)	85.3(4)	N(2)−Ta−N(1)	87.4(3)

Bond Angles (deg)

5		**7**	
C(1)−N(1)−C(11)	116.9(5)	C(1)−N(1)−C(11)	116.3(17)
C(11)−N(1)−Ta(1)	110.3(4)	C(11)−N(1)−Ta(1)	108.1(10)
C(1)−N(1)−Ta(1)	128.7(4)	C(1)−N(1)−Ta(1)	135.2(15)
C(9)−N(2)−C(14)	118.9(5)	C(10)−N(2)−C(14)	117(2)
C(9)−N(2)−Ta(1)	130.9(4)	C(14)−N(2)−Ta(1)	118.9(13)
C(14)−N(2)−Ta(1)	109.8(4)	C(10)−N(2)−Ta(1)	123.8(16)
N(1)−Ta(1)−N(2)	83.5(2)	N(2)−Ta(1)−N(1)	81.9(7)

We found that $TaMe_3Cl_2$ was a readily accessible and functional starting material to demonstrate both approaches. The direct reaction of the *N*,*N*′-diaryl-1,8-diaminonaphthalene with $TaMe_3Cl_2$ produced two analogous species $TaCl_3[1,8\text{-}(RN)_2C_{10}H_6]$ (**1** R = Ph; **2** R = 3,5-$Me_2C_6H_3$) as red-brown powders in good yields (Scheme 1). The ^{1}H NMR spectra for these compounds provided the first indication for the formation of the symmetrical structures for **1** and **2** as represented in Scheme 1. Specifically, the spectrum for **2** displayed a singlet, integrating for the 12 protons, consistent with four equivalent methyl groups on the N-Ar′ substituents. Furthermore, the simple ^{13}C NMR spectra for both **1** and **2** also suggested a symmetrical structure for both species. Importantly, neither complex displayed spectroscopic indications of remaining Ta-Me functions, suggesting that the reaction involved exchange of Cl and Me groups bonded to tantalum during the reaction. This is an established phenomenon.[4]

Details of the molecular connectivity and level of aggregation for **1** were revealed through X-ray crystallography (Table 1). These results are displayed in Figure 1 and summarized in Table 2. Examination of Figure 1 indicated that the coordination geometry for **1** is derived from a distorted trigonal-bipyramidal ligand array with two chloro ligands (Cl2 and Cl3) in the axial positions ($Cl_2-Ta-Cl_3$ = 169.0(1)°). The equatorial plane is defined by the remaining chloride (Cl1) and the N1 and N2 centers of the R_2DAN^{2-} ligand ($\sum$ angles = 360°). The two nitrogen centers (N1, N2) for the DAN ligand are planar ($\sum$ N angles 359.9° and 358.3°), and these planes are coincident with the plane of the naphthyl group, which aligns the lone pairs of electrons on these centers for π overlap with their adjacent atoms. The Ta−N bond lengths in **1** average 1.91 Å, while the Ta−Cl distances average 2.40 Å. A distinctive feature of the coordination of the diamidonaphthalene ligand to the Ta center is the planar orientation of the naphthyl moiety and the plane defined by N1−Ta−N2. While this is similar to our observations with Ge(II)[5] and our reported pnictogenium cations,[6] this observation differs significantly from the previously reported tungsten[3b] and tin[7] complexes bearing this ligand. For example, in the W(VI) complex $W(=N^tBu)_2[1,8\text{-}(^iPr\ N)_2C_{10}H_6]$ the naphthyl moiety and the N(1)−W(1)−N(2) plane exhibit a fold angle of 122.6°.

The starting material $TaMe_3Cl_2$ also represented an excellent choice for investigating a second approach for

(4) Fowles, G. W. A.; Rice, D. A.; Wilkins, J. D. *J. Chem. Soc., Dalton Trans.* **1973**, 961.

(5) Bazinet, P.; Yap, G. P. A.; Richeson, D. S. *J. Am. Chem. Soc.* **2001**, *123*, 11162.

(6) Spinney, H. S.; Korobkov, I.; DiLabio, G. A.; Yap, G. P. A.; Richeson, D. S. *Organometallics* **2007**, *26*, 4972.

(7) Bazinet, P.; Yap, G. P. A.; DiLabio, G. A.; Richeson, D. S. *Inorg. Chem.* **2005**, *44*, 4616.

introducing the R_2DAN^{2-} ligand (Scheme 1). The stoichiometric reaction of the *in situ* generated species $(R_2DAN^{2-})(Li^+)_2$ with one equivalent of $TaMe_3Cl_2$ led to the formation of $TaMe_3[1,8\text{-}(RN)_2C_{10}H_6]$ (R = Ph **3**; R = 3,5-$Me_2C_6H_3$ **4**) as dark orange and red materials, respectively. As with compounds **1** and **2**, complexes **3** and **4** displayed simple ^1H NMR spectra providing only one singlet for the three Ta-bonded methyl groups. Although this initially might suggest a symmetrical structure for **3**, structural analysis revealed nonequivalent methyl groups (*vide infra*). Therefore, the simplicity of the NMR spectra are likely a consequence of fluxionality of **3** and **4** on the NMR time scale. Finally, neither the ^1H nor ^{13}C NMR spectra indicated evidence of an α-agostic interaction of the Ta-Me groups.

Single crystals suitable for X-ray analysis where obtained for **3** from cooled solutions in diethyl ether (Table 1). These results, summarized in Figure 2 and Table 2, not only establish the connectivity for this compound but allow for comparison of this trimethyl species with the trichloro complex **1**. Similar to compound **1**, the Ta center of **3** resides in a distorted trigonal-bipyramidal coordination geometry. However, several key structural features of **3** contrast with those of **1**. Notably, in **3** the three methyl moieties are coordinated in a facial array and the DAN ligand is bonded to Ta through axial and equatorial sites, leading to the pseudoaxial positions being defined by a methyl group and one of the nitrogen centers of the DAN ligand (C24−Ta−N1 = 159.2(4)°). The equatorial positions are occupied by the remaining two methyl groups (C23, C25) and the second N center (N2) of the R_2DAN^{2-} ligand. The Ta−N bond lengths in **3** are slightly longer (~0.1 Å) than those observed for **1**. Furthermore the axial Ta−N bond length is, as anticipated, slightly longer (Ta−N1 = 2.064(7) Å) than the equatorial Ta−N2 bond at 1.954(7) Å. One of the most pronounced differences between the ligand binding in **3** compared to **1** is the orientation of the N-substituents relative to the naphthyl plane. Importantly, while the two N centers in the $(PhN)_2C_{10}H_6^{2-}$ ligand are planar with the sums of the angle around N1 and N2 being 360.0° and 359.4°, it is quite clear that the ligand in **3** is not planar. It is the relative orientation of the ligand components that clearly differentiates the DAN ligands of **1** and **3**. While $TaCl_3[1,8\text{-}(PhN)_2C_{10}H_6]$ (**1**) exhibited N planes that are coplanar with the naphthyl group, in the trimethyl complex **3**, only the plane for N1 is aligned with the napthyl moiety, while the N2 plane is almost perpendicular (77.2°) to the naphthyl plane. This orients the phenyl group bonded to N2 vertical to the ligand plane. As a result, the ligand in **3** is not coordinated to the Ta center in a planar fashion and the observed fold angle between the

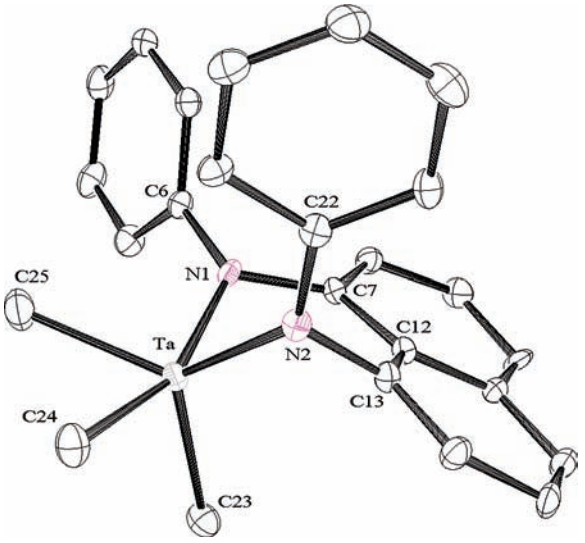

Figure 2. Thermal ellipsoid plot showing the molecular structure and partial atom-numbering scheme for $TaMe_3[1,8\text{-}(PhN)_2C_{10}H_6]$ (**3**). Ellipsoids are drawn at 20% probability. Hydrogen atoms have been omitted for clarity.

naphthyl moiety and the N_1-Ta-N_2 plane is 61.4°. This feature is reminiscent of the reported tungsten[3b] and tin[7] complexes with the R_2DAN^{2-} ligand. Furthermore, it is similar to structural features that have been observed in high-valent group 4,[1g] Ta,[8,9] Mo,[10] and W[11] species bearing *N*,*N*′-bis(trialkylsilyl)-*o*-phenylene diamide (PDA) ligands. In the case of the PDA complexes, the fold of the ligand about the N−N vector has been attributed to an increase in metal ligand interaction through a π donation from the phenylene component of the ligand into the metal orbitals.[8,10] In order to better understand the origin of these structural differences, we have examined **1** and **3** computationally, and the results of our analysis are presented below.

Similarly versatile Ta starting materials are represented by the two readily available Ta diethylamido species $\{Ta(NEt_2)_2Cl_3\}_2$ and the mononuclear analogue $Ta(NEt_2)_2Cl_3py$).[12] These species allow for further investigation of the role of the tantalum ligand scaffold on R_2DAN^{2-} bonding. Both of these starting complexes undergo metathesis reactions with an equimolar ratio of $Li_2(R_2DAN)$ to yield the analogous products $Ta[1,8\text{-}(RN)_2C_{10}H_6](NEt_2)_2Cl$ (R = $(CH_3)_2CH$ **5**, 3,5-$Me_2C_6H_3$ **6**) (Scheme 2), which were isolated as orange-red solids in 63% yield. The structure of $Ta(NEt_2)Cl[1,8\text{-}(^iPrN)C_{10}H_6]$ (**5**) was initially proposed on the basis of the ^1H NMR spectrum, which displayed single sets of resonances for the two diethyl amido groups and for two isopropyl groups on the DAN ligand. Significantly, the NMR data indicated that the ipso-CH signals of the isopropyl groups are intact in compound **5** and that both the ethyl CH_2 signals and the ipso-CH signals appeared as broad signals. These features point to two conclusions regarding **5**. First, in spite of the presence of basic amido sites within the tantalum complex, there is no reaction of these Ta-NR_2 groups with the isopropyl C−H bond. This contrasts with the reported reaction of $1,8\text{-}(^iPrNH)_2C_{10}H_6$ and

(8) Aoyagi, K.; Gantzel, P. K.; Tilley, T. D. *Polyhedron* **1996**, *15*, 4299.
(9) Pindado, G. J.; Thornton-Pett, M.; Bochmann, M. *J. Chem. Soc., Dalton Trans.* **1998**, 393.
(10) (a) Cameron, T. M.; Abboud, K. A.; Boncella, J. M. *Chem. Commun.* **2001**, 1224. (b) Ortiz, C. G.; Abboud, K. A.; Boncella, J. M. *Organometallics* **1999**, *18*, 4253.
(11) (a) Cameron, T. M.; Ortiz, C. G.; Abboud, K. A.; Boncella, J. M.; Baker, R. T.; Scott, B. L. *Chem. Commun.* **2000**, 573. (b) Wang, S. Y. S.; Vanderlende, D. D.; Abboud, K. A.; Boncella, J. M. *Organometallics* **1998**, *17*, 2628. (c) Wang, S. Y. S.; Abboud, K. A.; Boncella, J. M. *J. Am. Chem. Soc.* **1997**, *119*, 11990. (d) VanderLende, D. D.; Abboud, K. A.; Boncella, J. M. *Organometallics* **1994**, *13*, 3378.
(12) Chao, Y.-W.; Wexler., P. A.; Wigley., D. E. *Inorg. Chem.* **1989**, *28*, 3860.

Scheme 2

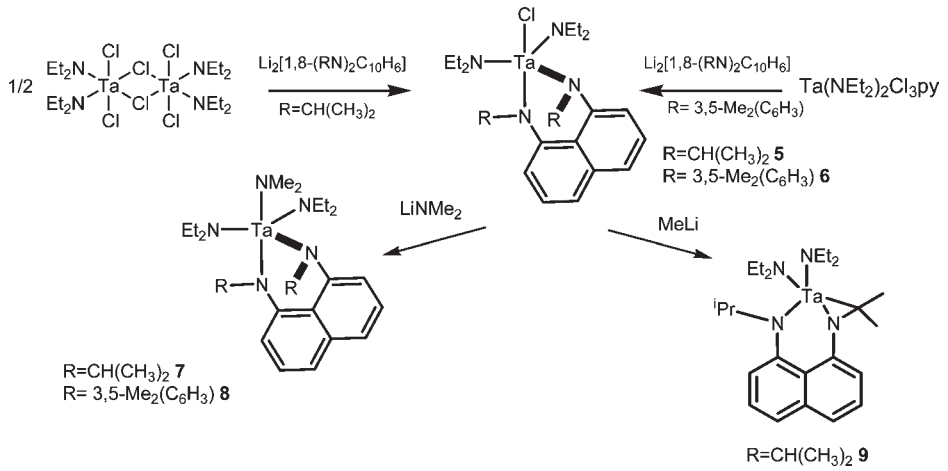

$TaMe_3Cl_2$, which involved the elimination of the isopropyl C−H bond and a Ta-Me group with formation of the metallaaziridine $[(Me_2CN)(Me_2CHN)(C_{10}H_6)TaCl_2]_2$.[3a] Second, complex **5** appeared to be fluxional on the NMR time scale at room temperature.

The connectivity of **5** was firmly established by X-ray crystallography (Table 1), with the results summarized in Figure 3 and Table 2. The Ta core is reminiscent of **3**, and, once again, the coordination geometry of the tantalum center can be described as a distorted trigonal bipyramidal with N(2) and Cl defining the axial positions (N(2)−Ta(1)−Cl(1) = 176.18(14)°). The sum of the angles in the equatorial plane defined by N1, N3, and N4 is 360°. The Ta−N1 and Ta−N2 bond lengths of 1.983(5) and 2.084(5) Å are comparable to reported complexes.[1a,3a] The Ta−NEt_2 bond lengths are slightly shorter at 1.948(5) Å (Ta−N3) and 1.965(5) Å (Ta−N4). Within the chelating $\{1,8\text{-}(^i\text{PrN})_2C_{10}H_6\}^{2-}$ ligand, nitrogen center N2 is planar, while N1 deviates very slightly from planarity ($\sum$ angles N1 = 355.9°). The plane of nitrogen N2 approaches alignment with the naphthyl plane. However, the mean plane for the N1 nitrogen makes an angle of 57° with the naphthyl plane. As a result, the isopropyl substituent on N1 points away from the napthyl plane. The overall coordination geometry and the relative orientation of the DAN ligand in **5** are similar to those observed in compound **3**.

Computational Studies of Complexes 1, 3, and 5. The fundamental electronic features that led to the observed structural differences for the trichloro complex **1** compared

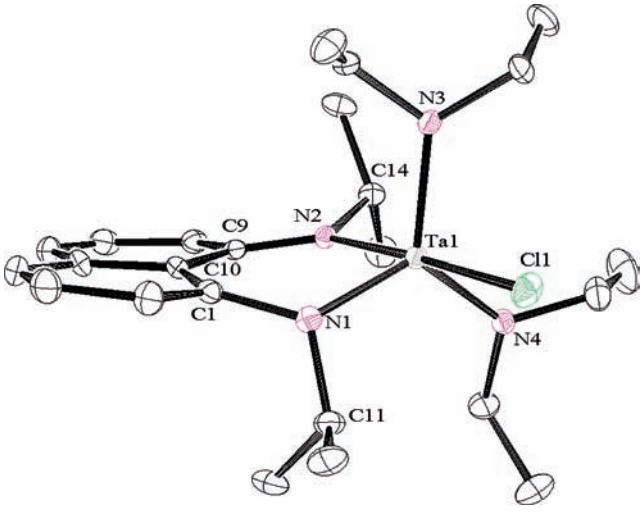

Figure 3. Thermal ellipsoid plot showing the molecular structure and partial atom-numbering scheme for $Ta(NEt_2)_2Cl[1,8\text{-}(N^iPr)_2C_{10}H_6]$ (**5**). Ellipsoids are drawn at 20% probability. Hydrogen atoms have been omitted for clarity.

to the trimethyl compound **3** and the amido compound **5** were examined computationally using density functional theory (DFT).[13] Optimizations of $[TaCl_3(1,8\text{-}(PhN)_2C_{10}H_6)]$ (**1**), $[TaMe_3(1,8\text{-}(PhN)_2C_{10}H_6)]$ (**3**), and $Ta(NEt_2)_2Cl[1,8\text{-}(N^iPr)_2C_{10}H_6]$ (**5**) using the B3LYP functional[14] with a LANL2DZ basis set[15] yielded computed structures that were similar to the experimental X-ray structures of these species in terms of metal coordination geometry, ligand orientation, and bond distances, thus supporting this approach. Our examination of these results begins with a comparison of the electronic features of **1** and **3** and is followed by inclusion of compound **5**.

In the case of compound **1** the computed structure displayed an R_2DAN^{2-} ligand with a planar coordination, as observed experimentally. An electronic analysis was first carried out by examination of the interaction of the diamido ligand $((PhN)_2C_{10}H_6)^{2-}$ fragment orbitals with those of the $TaCl_3^{2+}$ fragment.[16] The key donor orbitals of the ligand fragment are the four highest

(13) Frisch, M. J.; Trucks, G. W.; Schlegel, H. B.; Scuseria, G. E.; Robb, M. A.; Cheeseman, J. R.; Montgomery, J. A., Jr.; Vreven, T.; Kudin, K. N.; Burant, J. C.; Millam, J. M.; Iyengar, S. S.; Tomasi, J.; Barone, V.; Mennucci, B.; Cossi, M.; Scalmani, G.; Rega, N.; Petersson, G. A.; Nakatsuji, H.; Hada, M.; Ehara, M.; Toyota, K.; Fukuda, R.; Hasegawa, J.; Ishida, M.; Nakajima, T.; Honda, Y.; Kitao, O.; Nakai, H.; Klene, M.; Li, X.; Knox, J. E.; Hratchian, H. P.; Cross, J. B.; Bakken, V.; Adamo, C.; Jaramillo, J.; Gomperts, R.; Stratmann, R. E.; Yazyev, O.; Austin, A. J.; Cammi, R.; Pomelli, C.; Ochterski, J. W.; Ayala, P. Y.; Morokuma, K.; Voth, G. A.; Salvador, P.; Dannenberg, J. J.; Zakrzewski, V. G.; Dapprich, S.; Daniels, A. D.; Strain, M. C.; Farkas, O.; Malick, D. K.; Rabuck, A. D.; Raghavachari, K.; Foresman, J. B.; Ortiz, J. V.; Cui, Q.; Baboul, A. G.; Clifford, S.; Cioslowski, J.; Stefanov, B. B.; Liu, G.; Liashenko, A.; Piskorz, P.; Komaromi, I.; Martin, R. L.; Fox, D. J.; Keith, T.; Al-Laham, M. A.; Peng, C. Y.; Nanayakkara, A.; Challacombe, M.; Gill, P. M. W.; Johnson, B.; Chen, W.; Wong, M. W.; Gonzalez, C.; Pople, J. A. *Gaussian 03, revision C.02*; Gaussian, Inc.: Wallingford, CT, **2004**.

(14) Becke, A. D. *J. Chem. Phys.* **1993**, *98*, 5648. Lee, C.; Yang, W.; Parr, R. G. *Phys. Rev. B* **1988**, *37*, 785.

(15) Hay, P. J.; Wadt, W. R. *J. Chem. Phys.* **1985**, *82*, 299.

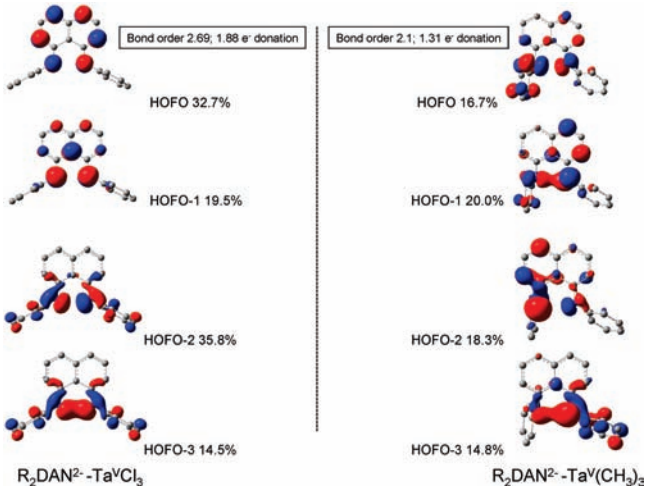

Figure 4. Highest occupied fragment orbitals (HOFOs) for the R_2DAN^{2-} ligand that participate in bonding with the $TaCl_3^{2+}$ fragment in complex **1** (left) and with the $Ta(CH_3)_3^{2+}$ fragment in complex **3** (right). The ligand−metal bond order and net electron donation as well as the change in occupancy for each HOFO are given.

occupied fragment orbitals (HOFOs) shown in Figure 4. The HOFO and HOFO−1 of the ligand participate in π donation to the metal fragment, and HOFO−2 and HOFO−3 participate in σ donation to the metal fragment. The changes in the orbital populations upon the formation of the complex are indicated by the percentage values next to each HOFO in the figure. Since these ligand orbitals are doubly occupied, charge donation from the ligand orbitals to the $TaCl_3^{2+}$ fragment can be evaluated. For example, the π donation from the interaction of the HOFO of the ligand with the unoccupied orbitals of the $TaCl_3^{2+}$ fragment is $0.327 \times 2 = 0.65$ electron. Adding contributions from all orbital interactions together, 1.88 electrons are donated from the R_2DAN^{2-} fragment to the $TaCl_3^{2+}$ fragment, giving a total bond order of 2.69. The donation from the ligand reduces the NPA charge[17] on Ta in the $TaCl_3^{2+}$ fragment from +1.75 to +1.54 au.

The optimization calculation for the trimethyl species **3** also reflected the orientation of the two amido moieties and the nonplanar orientation of the R_2DAN^{2-} ligand that was obtained from X-ray analysis. Again, the interactions of the diamido fragment, $((PhN)_2C_{10}H_6)^{2-}$, and the metal fragment $TaMe_3^{2+}$ were examined. The donor HOFOs for the ligand orientation represented in complex **3** are shown in Figure 4, and the energies of these fragment orbitals are similar to the orbital energies of those in **1**. The distortion from planarity changes the nature of the HOFOs to a mixture of σ and π overlap with the metal fragment. Again, the donor contribution from each ligand fragment orbital is shown by the percentage value of the change in electron population. Significant reduction in donation from the HOFO and HOFO−2 are the most important differences of **3** from **1**. With the nonplanar ligand orientation, the R_2DAN^{2-} fragment donates only 1.31 electrons to the $TaMe_3^{2+}$ fragment, and this in turn leads to a reduced bond order between the fragments of 2.10. The reduced donation is also reflected by the higher NPA charge on the Ta center in **3** of +1.97 au compared to **1**.

From this orbital interaction analysis it is clear that the degree of R_2DAN^{2-} donation and the ligand−metal fragment bond order is lower for the trimethyl complex **3** compared to the trichloro complex **1**. In order to determine the origin for these differences, the trimethyl complex $[TaMe_3(1,8\text{-}(PhN)_2C_{10}H_6)]$ (**3**) was examined with two different structural models. Specifically, the energy of the experimentally obtained structure for **3**, with a facial orientation of the Me groups, was compared to a model structure in which, analogously to complex **1**, positions of the methyl ligands were in a meridional array and a planar Ta-R_2DAN is maintained.[18] These two structures are displayed in Figure 5 along with their relative electronic energies. The relative energies for the two R_2DAN^{2-} ligand fragments of these species are also included in this figure. Interestingly, these results indicate that the planar geometry for the R_2DAN^{2-} fragment is slightly lower in energy (0.9 kcal mol^{-1}) than the nonplanar orientation that was observed in the experimental structure of **3**. More importantly, the electronic interaction energy between the R_2DAN^{2-} and $TaMe_3^{2+}$ fragments is 40.9 kcal mol^{-1} more negative (stable) for the planar ligand configuration than for the nonplanar configuration. However, the overall electronic energy of the nonplanar structure of **3** is 6.9 kcal mol^{-1} lower in energy than the model structure with the planar ligand and meridional methyl moieties.

These results directed our attention to the features that stabilize the facial orientation of the methyl groups in $TaMe_3^{2+}$ compared to the meridional chloro ligands in $TaCl_3^{2+}$ as the driving force for the determining the overall structures of **3** and **1**. A comparison of the energies for the two orientations of the methyl substituents in $TaMe_3^{2+}$ revealed that the facial disposition, experimentally observed for **3**, is 48.7 kcal mol^{-1} lower in energy than a meridional orientation of these groups in the model complex. The ultimate origin of this energy difference is revealed by examining the electrostatic interactions within the $TaMe_3^{2+}$ fragment. The C atoms of the methyl ligands in the $TaMe_3^{2+}$ fragment bear large negative charges (from −0.97 to −1.02 au). The electrostatic repulsion between these negative moieties results in the meridionally ligated $TaMe_3^{2+}$ lying 30.5 kcal mol^{-1} higher in energy than the facially ligated $TaMe_3^{2+}$ fragment. This electrostatic component appears to be the major contributor to stabilizing the experimentally observed structure of **3**.

A similar examination can be made for $[TaCl_3(1,8\text{-}(PhN)_2C_{10}H_6)]$, **1**. In this case, the electronic energy of a model structure of **1** with nonplanar R_2DAN^{2-} and facial chloro groups is 12.4 kcal mol^{-1} higher in energy than that of the experimentally observed structure. Similar to the $TaMe_3^{2+}$ fragment, the meridional $TaCl_3^{2+}$ fragment is 33.5 kcal mol^{-1} higher in energy than the computed facially ligated $TaCl_3^{2+}$ fragment. This indicates that the stabilizing energy for the observed

(16) Gorelsky, S. I.; Ghosh, S.; Solomon, E. I. *J. Am. Chem. Soc.* **2006**, *128*, 278. Gorelsky, S. I. *AOMix software for molecular orbital analysis*, www.sg-chem.net.

(17) Reed, A. E.; Weinstock, R. B.; Weinhold, F. *J. Chem. Phys.* **1985**, *83*, 735.

(18) The atomic coordinates for the optimized structures are provided in the Supporting Information.

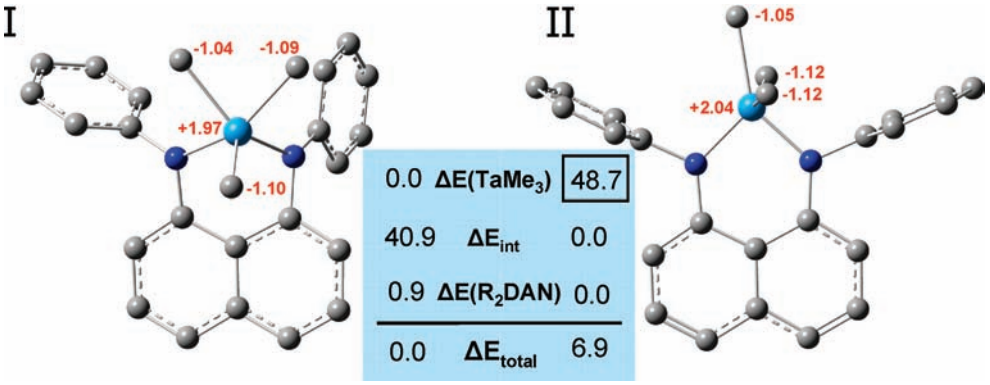

Figure 5. Comparison of the calculated energies for the experimental structure of **3** (I) and a model structure (II) for this compound. The hydrogen atoms on the two structures are omitted for clarity. The largest energy differences between these two isomers are the electronic interaction (ΔE_{int}) between the $TaMe_3^{2+}$ and R_2DAN^{2-} fragments and the relative energies between the two orientations of the $TaMe_3^{2+}$ fragments given by $\Delta E(TaMe_3)$. The difference in energy between the two R_2DAN^{2-} fragments is given by $\Delta E(R_2DAN)$. For reference, the charges on the Ta and Me centers are provided in red.

structure of **1** must originate from a different interaction than for **3**. In fact, the major stabilizing feature for complex **1** turns out to be the electronic interaction energy between the R_2DAN^{2-} and $TaCl_3^{2+}$ fragments. This interaction is 42.4 kcal mol^{-1} more negative for the planar ligand configuration than for the nonplanar configuration and arises from the stronger charge transfer interaction.

From these results we can conclude that the observed geometries of **1** and **3** are dictated by the balance between the energetics of the TaX_3^{2+} fragment and the TaX_3-R_2-DAN interaction energy. The loss of energy in distorting the DAN ligand from planarity is rather minor.

The similarity in the bonding array displayed by compound **5**, $[Ta(NEt_2)_2Cl(1,8\text{-}(^iPrN)_2C_{10}H_6)]$, to trimethyl compound **3** suggested that a similar electronic analysis of **5** should be carried out. Again the computed optimized structure for **5** at the B3LYP/DGDZVP level of theory was in accordance with the X-ray structure. The R_2DAN^{2-} ligand fragment of **5** displayed a set of donor HOFOs that correlated with the analogous fragment in **3**. The donation level of each of the ligand fragment frontier orbitals to the $Ta(NEt_2)_2Cl^{2+}$ fragment was very similar to what we observed in **3** with a total donation of 1.33 electrons, a bond order of 2.1, and a resulting NPA charge of +1.95 for the Ta(V) ion. The energy of this nonplanar ligand orientation is slightly higher than was observed for the nonplanar orientation observed for compound **3** and is 14.9 kcal mol^{-1} less stable than the planar R_2DAN ligand.

Calculations on a model structure of **5** with planar R_2DAN^{2-} and *mer*-$Ta(NEt_2)_2Cl$ ligand arrangement gave an electronic energy that was 20.8 kcal mol^{-1} higher in energy than that of the experimentally observed structure. As observed with **3**, the energy required to reorganize from the facial to the meridional $Ta(NEt_2)_2Cl^{2+}$ orientation is the dominant component for this increased energy. This *mer* orientation was computed to be 53.1 kcal mol^{-1} higher in energy than the *fac*-$Ta(NEt_2)_2Cl^{2+}$ fragment. Even though the planar R_2DAN^{2-} ligand would provide a more stabilizing interaction energy, by 17.5 kcal mol^{-1}, with the $Ta(NEt_2)_2Cl^{2+}$ fragment compared to the nonplanar configuration, this is not adequate to overcome the favored *fac*-$Ta(NEt_2)_2Cl^{2+}$ configuration.

Overall, these computational results correlate with experiment and demonstrate that the R_2DAN^{2-} ligand bonding configuration and the corresponding donation to the metal fragment is flexible. Significantly, the R_2DAN ligand−metal interactions respond to the demands of the Ta(V) fragment, which in turn is largely controlled by the nature of the ligands of the TaX_3^{2+} fragment.

Reactivity and Transformations of $Ta(NEt_2)_2Cl[1,8\text{-}(NR)_2C_{10}H_6]$ (R = ^{i}Pr 5; R = 3,5-$Me_2(C_6H_3)$ 6). The reactivity of compounds **5** and **6** provided an attractive avenue for exploring the stability and bonding of the R_2DAN^{2-} ligand coupled with the effects of metal coordination environment. Specifically, substitution of the chloro ligand of these species with both $LiNMe_2$ and LiMe was examined as summarized in Scheme 2. The reaction of either **5** or **6** with $LiNMe_2$ proceeded to introduce the dimethyl amido group on the tantalum center with elimination of LiCl and generation of compounds **7** and **8**. The ^1H and ^{13}C NMR spectra of these reaction products appear similar to the corresponding starting materials with the addition, in each case, of resonances corresponding to the incorporated dimethyl amido protons.

Suitable crystals for single-crystal X-ray diffraction analysis of $Ta(NEt_2)_2NMe_2[1,8\text{-}(^iPrN)_2C_{10}H_6]$ (**7**) were obtained from hexanes (Table 1). The results are summarized in Figure 6 and Table 2. Most striking is the similarity of **7** to the starting material **5** with the replacement of a chloro group with a dimethylamido ligand. The tantalum center remains in a distorted trigonal-bipyramidal coordination geometry with the R_2DAN^{2-} ligand spanning axial/equatorial sites (N1−Ta−N3 = 172.1(5)°) and with N2, N4, and N5 defining the equatorial plane ($\sum$ angles = 360°). The nitrogen centers of the R_2DAN^{2-} ligand are planar ($\sum$ angles N1 = 359.6°, $\sum$ angles N2 = 359.7°). The plane of nitrogen N1 approaches alignment with the naphthyl plane with the angle between these planes being only 21°. On the other hand, the mean plane for the N2 nitrogen makes an angle of 55° with the mean naphthyl plane. The net result is an R_2DAN^{2-} ligand geometry that is twisted and similar to that obtained in compound **5**.

A notable feature of **7** is that the ^{i}Pr groups of the DAN ligand remain intact in the formation of this compound. There is no deprotonation of the ispo-CH group even in the presence of three strongly basic amido ligands. This contrasts with the documented reactivity of the methyl

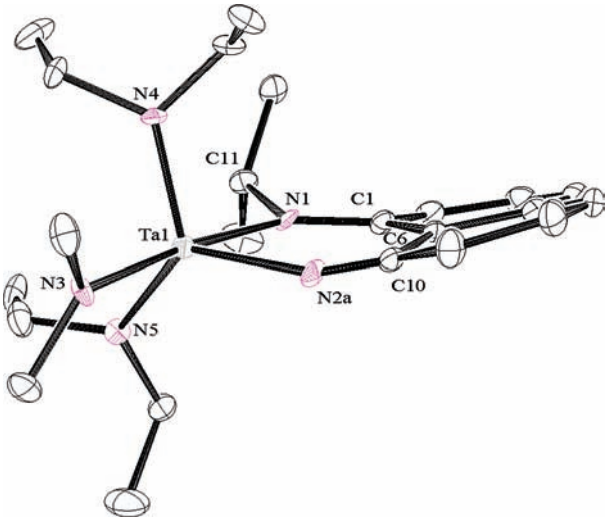

Figure 6. Thermal ellipsoid plot showing the molecular structure and partial atom-numbering scheme of $Ta(NEt_2)_2NMe_2[1,8\text{-}(^iPrN)_2C_{10}H_6]$ (**7**). Ellipsoids are drawn at 20% probability. Hydrogen atoms have been omitted for clarity.

groups in $TaMe_3Cl_2$ with $1,8\text{-}(^iPrNH)_2C_{10}H_6$, which ultimately led to metallaziridine via deprotonation of the isopropyl CH group.

These observations prompted our deployment of methyllithium in a reaction with $Ta(NEt_2)_2Cl[1,8\text{-}(^iPrN)_2C_{10}H_6]$ (**5**). The goal was to determine if this reaction would proceed by simple metathetical substitution of the chloro ligand with a methyl group or would involve transformation of the isopropyl CH group. From this reaction, an orange powder was obtained. Our previous experience with the appearance of the ^1H NMR spectrum for the tridentate trianionic metallaziridine ligand $(Me_2CN)(Me_2CHN)C_{10}H_6]^{3-}$ allowed us to rapidly identify compound **9** (Scheme 2) as the metallacyclic product. In particular, the spectrum for **9** displayed one intact ^{i}Pr group, exhibiting a doublet for the methyl moieties, and the methyl signals of the metallacycle appearing as a singlet with an integration value of six hydrogens. The remaining ^1H and ^{13}C NMR signals supported the structural assignment for $[(Me_2CN)(Me_2CHN)C_{10}H_6]Ta(NEt_2)_2$ (**9**).

Conclusions

A set of N,N′-disubstituted 1,8-diaminonaphthalenes have been employed in the preparation of a series of Ta(V) complexes with general formulas $(R_2DAN)TaX_3$. Characterization of these complexes allowed an examination of the influence of the R_2DAN ligand substituents as well as the influence of the other ligands on the structures and stability of the tantalum complexes. The use of aromatic substituents enabled the isolation of trichloro, trimethyl, and mixed bis(amido)/chloro Ta compounds with an analogous bis(amido)/chloro complex also being accessible with ^{i}Pr ligand substituents. While all of these species displayed distorted trigonal-bipyramidal Ta coordination geometries, there were significant differences in bonding of the R_2DAN^{2-} ligand to Ta and in the ligand orientation within the TaX_3^{2+} fragments.

A DFT computational analysis and modeling of the interaction between the R_2DAN^{2-} and TaX_3^{2+} fragments revealed that the distortion of the R_2DAN^{2-} ligand from planarity was a minor energy debt. Furthermore, the nonplanar ligand did exhibit a lower $R_2DAN-TaX_3$ interaction energy, which led to reduced electron donation from the ligand and diminished bond order between the ligand and Ta. In opposition to these destabilizing features was a rather large energy contribution favoring a facial arrangement of the ligands in the TaX_3^{2+} fragments. Interestingly, the balance of these energy terms demonstrated the flexibility of the R_2DAN^{2-} ligand in bonding to a metal center and the responsiveness of this donor species to the demands of the Ta(V) fragment, TaX_3^{2+}, which in turn was dictated by the nature of the groups constituting this fragment.

Finally, the substitution reactions of the chloro ligand in $Ta(NEt_2)_2Cl[1,8\text{-}(^iPrN)_2C_{10}H_6]$ (**5**) provided a probe for the σ-bond metathesis transformation of the Ta-$NCHMe_2$ moiety into a metallaziridine κ^2-(Me_2CN)Ta. This conversion was observed in the reaction of **5** with MeLi but not with $LiNMe_2$.

Experimental Section

General Methods. All manipulations were carried out either in a nitrogen-filled drybox or under nitrogen using standard Schlenk line techniques. Unless otherwise noted, solvents were sparged with nitrogen and then dried by passage through a column of activated alumina using an apparatus purchased from Anhydrous Engineering. Deuterated benzene and methylene chloride were dried by vacuum transfer from molecular sieves. $TaCl_5$ was purchased from Strem and used without further purification. *N*,*N*-Diethyltrimethylsilylamine was purchased from Aldrich and used without further purification. ^1H NMR spectra were recorded at room temperature and run on either a Bruker Avance 300 MHz or a Bruker 500 MHz spectrometer with deuterated benzene or methylene chloride as a solvent and internal standard. Elemental analyses were carried out by Robertson Microlit Laboratories, Inc. (Madison, NJ) or Midwest Microlab, LLC (Indianapolis, IN). Multiple attempts to obtain microanalyses of compounds **1**−**4** were unsuccessful. Samples of these compounds changed color from orange to dark brown during overnight shipping. $[Ta(NEt_2)_2Cl_3]$,[12] $Ta(NEt_2)_2Cl_3Py$,[12] $1,8\text{-}(2,6\text{-}Me_2C_6H_3NH)_2C_{10}H_6$,[19] $1,8\text{-}(NH^iPr)_2C_{10}H_6$, and $TaMe_3Cl_2$[20] were prepared according to literature methods.

Preparation of $TaCl_3[1,8\text{-}(Ph)_2C_{10}H_6]$ (1). A dark brown solution was formed after stirring $1,8\text{-}(C_6H_5NH)_2C_{10}H_6$ (0.191 g, 0.64 mmol) and $TaMe_3Cl_2$ (0.201 g, 0.65 mmol) in 10 mL of diethyl ether under nitrogen for 24 h. Ether was removed under vacuum from the reaction mixture, and the solid was extracted with 4 mL of toluene. Addition of hexanes to this solution and cooling to −20 °C gave red crystals (0.151 g, 39.6%) of compound **1**.

^1H NMR (300 MHz, C_6D_6): δ 6.38 (d, 2H), 7.02 (m, 6H), 7.19 (m, 2H), 7.23(m, 2H), 7.80 (m, 4H). ^{13}C NMR (300 MHz, C_6D_6): δ 115.5 (CH_{Ar}), 125.6 (C_{Ar}), 126.6 (C_{Ar}), 127.3 (CH_{Ar}), 128.5 (CH_{Ar}), 129.2 (CH_{Ar}), 129.3 (CH_{Ar}), 132.9 (C_{Ar}), 134.2 (CH_{Ar}), 135.5 (C_{Ar}).

Preparation of $TaCl_3[1,8\text{-}(3,5\text{-}Me_2C_6H_3N)_2C_{10}H_6]$ (2). In a nitrogen-filled glovebox, $TaMe_3Cl_2$ (0.243 g, 0.82 mmol) and $1,8\text{-}(3,5\text{-}Me_2C_6H_3NH)_2C_{10}H_6$ (300 mg, 0.82 mmol) were dissolved in toluene, and the reaction mixture was allowed to stir overnight at room temperature. The resulting red solution was dried by vacuum evaporation of the reaction solvent. A brown powder was obtained, which was dissolved in hexanes cooled to −20 °C to give a red powder of **2** (269 mg, 51.0%).

(19) Bazinet, P.; Ong, T. G.; O'Brien, S. J.; Lavoie, N.; Bell, E.; Yap, G. P. A.; Korobkov, I.; Richeson, D. S. *Organometallics* **2007**, *26*, 2885.
(20) Juvinall, G. L. *J. Am. Chem. Soc.* **1964**, *86*, 4202.

^{1}H NMR (300 MHz, C_6D_6): δ 2.02 (s, 12H, CH_3), 6.45 (s, 2H, CH_{Ar}) 6.55 (s, 4H, CH_{Ar}), 7.18−7.27 (m, 4H, CH_{Ar}), 7.43 (d, 2H, CH_{Ar}). ^{13}C NMR (500 MHz, CD_2Cl_2): δ 21.6 (CH_3), 116.8 (CH_{Ar}), 117.4 (CH_{Ar}), 122.2 (C_{Ar}), 123.6 (CH_{Ar}), 126.5 (C_{Ar}), 126.6 (CH_{Ar}), 137.7 (C_{Ar}),139.5 (CH_{Ar}), 141.3 (C_{Ar}), 145.4 (C_{Ar}).

Preparation of $TaMe_3$[1,8-$(Ph)_2C_{10}H_6$] (3). In a nitrogen-filled glovebox, 1,8-$(C_6H_5NH)_2C_{10}H_6$ (0.62 g, 2 mmol) was dissolved in 5 mL of diethyl ether and cooled to −30 °C. To this solution was added dropwise methyllithium (2.9 mL of a 1.4 M solution in diethyl ether, 4.06 mmol). The reaction mixture was maintained at −30 °C and stirred for 30 min. $TaMe_3Cl_2$ (0.59 g, 1 mmol), which had been dissolved in 5 mL of diethyl ether, was then added slowly to the reaction mixture. This mixture was allowed to stir for 1 h at room temperature. After filtration, the resulting dark red solution was cooled to −30 °C. Dark orange crystals of **3** were obtained after several hours (0.31 g, 29%).

^{1}H NMR (300 MHz, C_6D_6): δ 1.20 (s, 9H), 6.73 (m 2H), 6.95 (m, 4H), 7.06 (m, 2H), 7.18 (m, 6H), 7.24 (m, 2H). ^{13}C NMR (300 MHz, C_6D_6): δ 75.3 (CH_3), 120.1 (CH_{Ar}), 123.9 (CH_{Ar}), 125.2 (CH_{Ar}), 125.8 (CH_{Ar}), 126.4 (C_{Ar}), 129.5 (C_{Ar}), 130.2 (CH_{Ar}), 137.0 (C_{Ar}), 143.1 (C_{Ar}), 146.4 (CH_{Ar}).

Preparation of $TaMe_3$[1,8-$(3,5\text{-}Me_2C_6H_3N)_2C_{10}H_6$] (4). In a round-bottom flask 1,8-$(3,5\text{-}Me_2C_6H_3NH)_2C_{10}H_6$ (300 mg, 0.82 mmol) was dissolved in diethyl ether at room temperature. To this solution was added dropwise ^{n}BuLi (1.02 mL of 1.6 M solution in ether, 1.6 mmol). The reaction mixture was allowed to stir for 1 h. $TaMe_3Cl_2$ (0.243 g, 0.82 mmol) was then added slowly to the reaction flask. The reaction mixture was then stirred for an additional 3 h and filtered, and the solvent was evaporated under vacuum to yield a brown solid. Compound **4** was purified by precipitation from toluene (208 mg, 89%).

^{1}H NMR (300 MHz, C_6D_6): δ 1.24 (s, 9H, Me), 1.98 (s, 12H, Me) 6.60 (s, 2H, CH_{Ar}), 6.80 (s, 4H, CH_{Ar}), 6.87 (d, 2H, CH_{Ar}), 7.15−7.27 (m, 4H, CH_{Ar}). ^{13}C NMR (300 MHz, C_6D_6): δ 21.4 ($C_{Ar}CH_3$), 73.6 (TaCH_3), 119.2 (C_{Ar}), 123.8 (CH_{Ar}), 123.9 (CH_{Ar}), 126.5 (C_{Ar}), 127.7 (CH_{Ar}), 127.8 (CH_{Ar}), 137.4 (C_{Ar}), 140.3 (CH_{Ar}), 144.4 (C_{Ar}), 144.7 (C_{Ar}).

Preparation of $Ta(NEt_2)_2Cl$[1,8-$(N^iPr)_2C_{10}H_6$] (5). In a round-bottom flask 1,8-$(^iPrNH)_2C_{10}H_6$ (0.50 g, 2.06 mmol) was dissolved in diethyl ether at room temperature. To this solution was added dropwise ^{n}BuLi (2.58 mL of a 1.6 M solution in diethyl ether, 4.13 mmol). The reaction mixture was allowed to stir for 1 h. $[Ta(NEt_2)_2Cl_3]_2$ (0.89 g, 1.03 mmol) was then added to the reaction flask. This mixture was then allowed to stir overnight and filtered through Celite, and the solvent was evaporated under vacuum. The resulting orange solid was recrystallized from hexanes cooled to −20 °C to yield **5** (0.782 g, 63.2%) as orange crystals.

^{1}H NMR (300 MHz, C_6D_6): δ 0.88 (t, 12H, NCH_2CH_3), 1.25 (d, 12H, $CH(CH_3)_2$), 3.62−3.44 (br, 8H, NCH_2CH_3), 4.67−4.24 (br, 2H, $CH(CH_3)_2$), 6.75−7.14 (m, 2H, Ar-H), 7.26−7.47 (m, 4H, Ar-H). ^{13}CNMR (300 MHz, C_6D_6): δ 13.8 (NCH_2CH_3), 21.7 ($CHCH_3$), 45.8 (NCH_2CH_3), 50.4 ($CH(CH_3)_2$, 55.3 (CH-$(CH_3)_2$, 113.6 (C_{Ar}), 119.5 (C_{Ar}), 124.3 (C_{Ar}), 126.1 (CH_{Ar}), 128.9 (CH_{Ar}), 137.2 (CH_{Ar}). Anal. Calcd for $C_{24}H_{40}N_4ClTa$: C 47.96, H 6.71, N 9.32 Found: C 47.69, H 6.43, N 9.16

Preparation of $Ta(NEt_2)_2Cl$[1,8-$(3,5\text{-}Me_2C_6H_3N)_2C_{10}H_6$] (6). In a round-bottomed flask 1,8-$(3,5\text{-}Me_2C_6H_3NH)_2C_{10}H_6$ (0.5 g, 1.36 mmol) was dissolved in diethyl ether at room temperature. To this solution was added dropwise ^{n}BuLi (1.71 mL of a 1.6 M solution in diethyl ether, 2.7 mmol). The reaction mixture was allowed to stir for 1 h. $Ta(NEt_2)_2Cl_3Py$ (0.697 g, 1.36 mmol) was then added to the reaction flask. This mixture was then allowed to stir overnight and filtered through Celite, and the solvent was evaporated under vacuum. The resulting red solid was recrystallized from hexanes cooled to −20 °C to yield **6** (612 mg, 62.5%).

^{1}H NMR (300 MHz, C_6D_6): δ 0.65 (t, 12H, NCH_2CH_3), 2.05 (12H, s, $C_{Ar}CH_3$), 3.60 (q, 8H, NCH_2CH_3), 6.57 (s, 2H, Ar-H), 6.73 (br, 2H, Ar-H), 7.06−7.14 (br, 4H, Ar-H), 7.17−7.25 (m, 4H, Ar-H). ^{13}C NMR (300 MHz, C_6D_6): δ 13.0 (NCH_2CH_3), 21.5 ($C_{Ar}CH_3$), 45.6 (NCH_2CH_3), 117.1 (CH_{Ar}), 117.5 (C_{Ar}), 123.8 (C_{Ar}), 125.7 (CH_{Ar}), 126.5 (C_{Ar}), 126.7 (CH_{Ar}), 127.5 (CH_{Ar}), 129.5 (C_{Ar}), 136.9 (C_{Ar}), 139.2 (CH_{Ar}). Anal. Calcd for $C_{34}H_{44}N_4ClTa$: C 56.32, H 6.12, N 7.73. Found: C 56.53, H 6.21, N 7.59.

Preparation of $Ta(NEt_2)_2NMe_2$[1,8-$(N^iPr)_2C_{10}H_6$] (7). In a round-bottomed flask, compound **5** (0.18 g, 0.30 mmol) was dissolved in 40 mL of diethyl ether. To this solution was added $LiNMe_2$ (0.015 g, 0.30 mmol), and the reaction mixture was allowed to stir overnight. The reaction mixture was filtered, and the solvent was removed under vacuum. Orange crystals of **7** (117 mg, 65.1%) were obtained by recrystallization from hexanes cooled to −20 °C.

^{1}H NMR (300 MHz, C_6D_6): δ 0.90 (t, 12H, NCH_2CH_3), 1.26 (d, 12H, $CH(CH_3)_2$), 3.35 (s, 6H, NCH_3), 3.39 (q, 4H, NCH_2CH_3), 3.68 (q, 4H, NCH_2CH_3), 4.16 (sept, 2H, $CH(CH_3)_2$), 6.96−6.99 (m, 2H, Ar-H), 7.34−7.38 (m, 4H, Ar-H). ^{13}C NMR (300 MHz, C_6D_6): δ 14.5 (NCH_2CH_3), 23.6 ($CHCH_3$), 46.4 (NCH_3), 48.6 (NCH_2CH_3), 51.6 ($CH(CH_3)_2$), 115.2 (C_{Ar}), 119.8 (C_{Ar}), 125.8 (CH_{Ar}), 128.8 (CH_{Ar}), 137.7 (CH_{Ar}), 147.7 (C_{Ar}). Anal. Calcd for $C_{32}H_{42}N_5Ta$: C 51.22, H 7.62, N 11.49. Found: C 50.74, H 7.27, N 11.15.

Preparation of $Ta(NEt_2)_2NMe_2$[1,8-$(2,6\text{-}Me_2C_6H_3N)_2C_{10}H_6$] (8). In a round-bottom flask, compound **6** (0.765 g, 1.05 mmol) was dissolved in 40 mL of diethyl ether. To this solution was added $LiNMe_2$ (0.057 g, 1.12 mmol), and the reaction mixture was allowed to stir overnight. The reaction mixture was filtered, and the solvent was removed under vacuum. Orange crystals of **8** (0.607 g, 78.8%) were obtained by recrystallization from hexanes and THF.

^{1}H NMR (300 MHz, C_6D_6): δ 0.64 (t, 12H, NCH_2CH_3), 2.15 (s, 12H, $C_{Ar}CH_3$), 3.01 (s, 6H, $N(CH_3)_2$), 3.31 (q, 4H, NCH_2CH_3), 3.81 (q, 4H, NCH_2CH_3), 6.58 (s, 4H, Ar-H), 6.71 (s, 4H, Ar-H), 7.14−7.30 (m, 4H, Ar-H). ^{13}C NMR (300 MHz, C_6D_6): δ 14.4 (NCH_2CH_3), 21.7 ($C_{Ar}CH_3$), 46.1 (N(CH3)), 47.8 (NCH_2CH_3), 115.0 (C_{Ar}), 119.6 (C_{Ar}), 124.8 (CH_{Ar}), 124.9 (C_{Ar}), 125.2 (CH_{Ar}), 127.3 (CH_{Ar}), 128.2 (C_{Ar}), 137.9 (C_{Ar}), 138.6 (CH_{Ar}), 151.3 (C_{Ar}), 153.4 (CH_{Ar}). Anal. Calcd for $[C_{36}H_{50}N_5Ta]\cdot 2[THF]$: C 60.19, H 7.58, N 7.98. Found: C 60.59, H 7.49, N 8.24.

Preparation of η^3-$C_{10}H_6(Me_2CN)(Me_2CHN)Ta(NEt_2)_2$ (9). In a round-bottomed flask, compound **5** (469 mg, 0.78 mmol) was dissolved in 30 mL of diethyl ether. To this solution was added MeLi (0.49 mL of a 1.6 M solution in diethyl ether (0.78 mmol)), and the reaction mixture was allowed to stir overnight. The reaction mixture was filtered, and the solvent was removed under vacuum to give an orange solid. Orange crystals of **9** (224 mg, 50.8%) were obtained by recrystallization from ether at −20 °C.

^{1}H NMR (300 MHz, C_6D_6): δ 0.83 (t, 12H, NCH_2CH_3), 1.57 (d, 6H, $CH(CH_3)_2$), 2.16 (s, 6H, $C(CH_3)_2$, 3.02 (br, 8H, NCH_2CH_3), 4.47 (sept, 1H, $CH(CH_3)_2$), 6.90−6.96 (m, 2H, Ar-H), 7.34−7.47 (m, 4H, Ar-H). ^{13}C NMR (300 MHz, C_6D_6): δ 16.7 (NCH_2CH_3), 21.8 (CH_3), 27.4 (CH_3), 42.6 (NCH_2CH_3), 52.6 ($CH(CH_3)_2$), 107.0 (CH_{Ar}), 109.1 (CH_{Ar}), 118.8 (CH_{Ar}), 125.3, (CH_{Ar}), 126.3 (CH_{Ar}), 126.7 (CH_{Ar}), 128.7 (CAr), 129.9 (CAr), 139.1 (C_{Ar}), 145.3 (C_{Ar}). Anal. Calcd for $C_{24}H_{39}N_4Ta$: C 51.06, H 6.96, N 9.92. Found: C 50.93, H 6.84, N 9.84.

Computational Details

DFT calculations with the B3LYP functional were carried out using the Gaussian 03 (revision D.01) suite of programs. Spin-restricted treatment was used for all closed-shell species. The basis set LANL2DZ was employed. Atomic charges were calculated by natural population analysis (NPA) as implemented in Gaussian 03. Mayer

bond orders were obtained using the AOMix-L program. The analysis of molecular orbitals (MOs) in terms of fragment orbital (FO) contributions and calculations of the FO overlap matrices and FO populations were carried out using the AOMix-CDA program. The converged wave functions were tested to confirm that they represent the true ground state.

Acknowledgment. This work was supported by the NSERC of Canada.

Supporting Information Available: Atomic coordinates for the optimized experimental and model structures of **1**, **3**, and **5**. Crystallographic files (cif) for compounds **1**, **3**, **5**, and **7**. This material is available free of charge via the Internet at http://pubs.acs.org.